Eur. Phys. J. Spec. Top. (2022) 231:589–595
https://doi.org/10.1140/epjs/s11734-021-00382-9

THE EUROPEAN PHYSICAL JOURNAL SPECIAL TOPICS

Regular Article

Tunable TE/TM mode converter with an orthogonal graphene-based grating structure

Yiqing Wang[1], Wenjie Shi[1], Qian Li[1], Yifan Chen[1], Jicheng Wang[1,2,a], and Wei Liu[3,b]

[1] School of Science, Jiangsu Provincial Research Center of Light Industrial Optoelectronic Engineering and Technology, Jiangnan University, Wuxi 214122, China
[2] State Key Laboratory of Applied Optics, Changchun Institute of Optics, Fine Mechanics and Physics, Chinese Academy of Sciences, Changchun 130033, China
[3] School of Electronic and Information Engineering, Harbin Institute of Technology, Shenzhen 518055, Guangdong, China

Received 8 April 2021 / Accepted 13 December 2021 / Published online 13 January 2022

Abstract A novel TM/TE polarization converter constructed with orthogonal double-layer graphene gratings is proposed. The high-performance TM/TE polarization conversion was explored by optimizing the Fermi energy and geometric parameters of the two-layer graphene gratings. As the Fermi level of graphene is dynamically adjustable, tunable polarization modulation can be achieved by the same design. Here we utilize the finite element method and improved coupled-mode theory to simulate and verify the conversion and modulation characteristics of TM and TE polarization. Proof-of-concept experiments demonstrated that this TM/TE converter provided excellent optical efficiency in polarization conversion and strong modulation stability against incident wave angle (up to 30°) and polarization status. This simple and easy-to-implement grating structure paves the way for the development of future micro-nano devices such as unimodal filters, and its functions can be further translated to study absorption and reflection spectra in nanophotonic applications.

1 Introduction

The optical waveguide circuit is expected to play a crucial role in the optical communication systems. In recent years, polymer electro-optic waveguide devices have been of interest to researchers, and many thin-film waveguide circuits have been successfully demonstrated [1, 2]. Similarly, polarization-independent optical metasurfaces have made some progress, provide a new method for the designs of optical hypersurface equipment [3–5]. Non-reciprocal devices such as isolators and circulators are also needed when building optical signal processing systems. Although bulk non-reciprocal devices use a continuous rotation of linear polarized light planes, waveguide devices must be based on TE–TM mode conversion. TE/TM converter is a key component used to operate the polarization state of light wave. There are many mode conversion technologies, such as the waveguide method, photon lantern method, pure phase spatial light modulator method and so on. High focus application of beam deflector in mid-infrared band has also made the wave switch more significant in the optical field. Jafari et al. proposed a silicon optical modulator, achieved low loss reflection modulation without circulator using asymmetric Bragg gratings [6]. In addition, the mode converter is the building block of polarization diversity configuration, which enables it to construct polarization-independent circuit [7]. The first passive TE/TM mode converter has been shown to use asymmetric periodic loaded rib waveguide and transversely tilted periodic rib waveguide.

Graphene is a two-dimensional crystalline structure of carbon atoms. It has significant electronic properties, and its Fermi energy can be adjusted by changing chemical doping or electrostatic gating, its fermi velocity of graphene can fully control its transport characteristics. So that we can achieve a large dynamic tuning of its surface conductivity. Due to its excited electron transport properties, graphene has important and extensive applications in ultra-compact devices [8] in the infrared [9, 10] and terahertz (THz) bands [11–13]. Graphene has extremely high carrier mobility at room temperature, and has strong mode constraints and low propagation loss for surface plasmon polaritons (SPPs) [14] in the infrared band [15]. In addition, under the condition of applying an external bias voltage, the carrier mobility of graphene can be modulated on the order of nanoseconds. These properties make graphene an excellent material for preparing electrically tunable plasma devices [16–19]. The unique photoelectric properties of graphene provide the possibility for its extensive applications in the field of optical waveguide. Nowadays,

[a] e-mail: jcwang@jiangnan.edu.cn (corresponding author)
[b] e-mail: wl157@hit.edu.cn (corresponding author)

there have been many fruitful results in the study of mode coupling in the metal/dielectric plate composite structure [20–22], and the graphene plasmon effect has also become a very popular field [23, 24]. If we make full use of the characteristics of both two mentioned above to realize a grating modulation [25], there will be more people to study the mode coupling and light control characteristics of this structure, and more new effects and new properties will be discovered [26]. However, the modulation that achieves TE or TM polarization coupling with graphene-based multiple orthogonal gratings has rarely been studied.

In this paper, we propose an elaborate TM/TE converter composed of orthogonal graphene-based gratings. This converter realizes mode switch by rotating the top layer 90° to make the two gratings perpendicular to each other. Monolayer graphene is placed at the bottom of the grating, we can perfectly achieve single-peak filtering by changing the graphene's Fermi energy for its optical response tunability. When the TM-polarized wave is incident from either side of the device, it can excite the magnetic resonance (MR) of the structure; thus, forming a transmission valley, and the transmitted electromagnetic wave has the TE polarization state. Meanwhile, changing the geometric parameters of the grating also has an impact on the filtering properties. We explore this effect of configuration parameter on transmission spectrum by finite element method and the coupled-mode theory (CMT), we come to the conclusion that the numerical simulation data are perfectly consistent with the theory. Additionally, the incident angle insensitivity and bidirectional incident ability of the structure also provide a basis for its wide application in other fields.

2 Structure and methods

As shown in Fig. 1a, a TM/TE polarization switch is constructed based on bilayer orthogonal gratings. We use the finite element method (FEM) to explore the filter performance. The structure consists of three parts: the upper graphene-based grating layer, the intermediate dielectric spacer layer, and the lower graphene-based grating layer. The grating is composed of ZnSe substrates and the dielectric constant of ZnSe is a semiconductor material [14] with excellent photoelectric properties, it has low scattering in its commonly used spectral range. ZnSe crystal material has become the preferred material for making optical devices in high power CO_2 laser system because of its small absorption of 10.6 wavelength light. ZnSe material is highly applied in laser, astronomical, infrared night vision, medical, measurement, industrial, military and high-tech fields [27, 28]. The substates of the proposed grating device are made of ZnSe, which is a kind of semiconductor material in high-tech fields, and in our simulation, we set its dielectric to 2.4. We assume that graphene monolayer is a two-dimensional conductive surface with zero thickness, which absorptivity can reach 2.3%. The bidirectional incidentable character of the structure reflects the superiority of mode coupling, when the TM polarization is irradiated from the upper grating, it can be converted into TE polarization by passing through the orthogonal grating system. Optimizing the structure, the width of the upper grating is set to $w\_r1 = 45$ nm, the width of the lower grating is set to $w\_r2 = 90$ nm, the grating period is $W = 120$ nm, the thickness of the substrate is $D = 50$ nm. Theoretically, the spectrum can be filtered with transmission close to 0. The height of the grating has no effect on the transmission valley, so we set it to a constant $d = 100$ nm. Polarized wave with an electric vector perpendicular to the incident plane is called the TE wave, and a polarized wave whose electric vector is parallel to the incident plane is called the TM wave. The polarization conversion diagram is represented in Fig. 1b. The polarization direction is irrevocable when the TM-polarized wave irradiates and passes through the first narrow grating. However, the other grating is vertical to the upper one. As the TM wave incident into the surface of the lower grating, it converts to TE polarization relative to the orthogonal grating. It can be seen that the light wave itself does not change, and the orthogonal combination mode of the gratings causes the relative polarization direction conversion. To obtain efficient and accurate data, adaptive mesh is used in numerical simulation and local mesh refinement is carried out. The continuous graphene layers are placed below the wide grating and the narrow grating, respectively, as surface current density conditions.

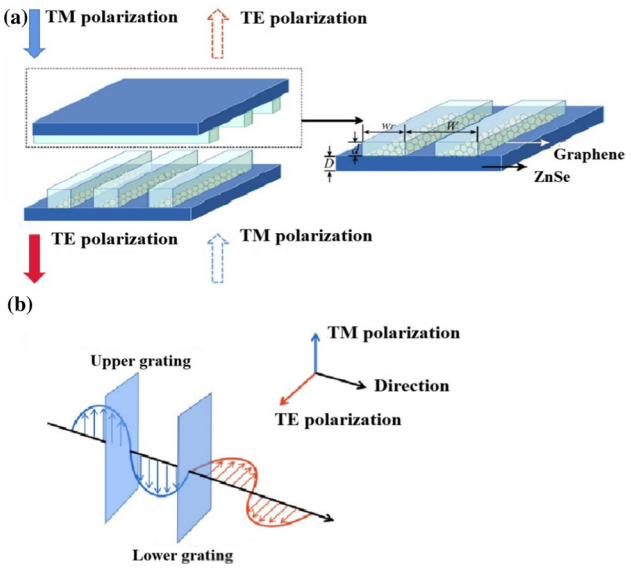

Fig. 1 **a** Schematic of the graphene grating system formed by two layers of orthogonal gratings. System parameters include D, d, wr, W, which refer to the ZnSe substrate thickness, the height of the grating, the width of the grating and the system period. **b** Conversion schematic of TM polarization and TE polarization

By regulating the Fermi energy (E_F) of graphene, its optical response tunability can be flexibly controlled. The conductivity of graphene can be expressed as the sum of inter-band and intra-band contributions [29, 30].

$$\sigma = \sigma_{\text{intra}} + \sigma_{\text{inter}}, \tag{1}$$

More precisely, the intar-band part is given by

$$\sigma_{\text{intra}}(\omega, E_F, \tau, T) = -\frac{ie^2(\omega + i\tau^{-1})}{\pi\hbar^2}\int_{-\infty}^{+\infty}\frac{|\xi|}{(\omega + i\tau^{-1})^2}\frac{\partial f_d(\xi)}{\partial \xi}d\xi, \tag{2}$$

$$\sigma_{\text{inter}}(\omega, E_F, \tau, T) = \frac{ie^2(\omega + i\tau^{-1})}{\pi\hbar^2}\int_{0}^{+\infty}\frac{\partial f_d(-\xi) - \partial f_d(\xi)}{(\omega + i\tau^{-1})^2 - 4(\xi/\hbar)^2}d\xi. \tag{3}$$

In the above equation, f_d represents Fermi–Dirac distribution.

$$f_d = \frac{1}{1 + \exp\left(\frac{\xi - E_F}{k_B T}\right)}, \tag{4}$$

where E_F is the Fermi energy, e is electric charge, ξ is energy, T is temperature, $\hbar$ is reduced Planck constant, $\tau = \mu E\_F/(ev^2F)$ represents carrier relaxation time, μ is carrier mobility[31], $v\_F = 10^8$ cm/s represents Fermi velocity.

From the above equation, it can be seen that the conductivity of intra-band and inter-band transition is closely related to the Fermi energy of graphene [32]. Moreover, the Fermi energy of doped graphene is determined by the carrier concentration. Graphene has unique carriers, not only its concentration can be regulated by chemical doping or external electromagnetic field, but also its mobility is particularly high. The experiment shows that the carrier mobility can be as high as 37,000 $\text{cm}^2\text{V}^{-1}\ \text{s}^{-1}$. During the numerical study, it is found that the graphene grating filtering performance is better when the carrier mobility is around 25,000 $\text{cm}^2\text{V}^{-1}\ \text{s}^{-1}$.

There are many theories about resonators [33], among which the transmission matrix method [34, 35] is celebrated. It is intuitionistic and the physical meaning is clear when dealing with coupling between modes. However, in the process, different coupling points need to be segmented, and at least two variables are needed to represent the incident and reflected waves in each segment. There are so many variables to deal with that the calculation is a bit complicated. Coupled mode theory (CMT) [36–38] can analyze the transmittance characteristics of the system, which only needs to consider the mode in the resonator that greatly simplifies the processing process.

As depicted in Fig. 2, the double resonator system is proposed. M represents the incident or outgoing waves of the dual-coupled resonator. The superscript and subscript are used to distinguish the incoming, outgoing or propagating direction of the wave. The in means the incident wave while the out means the outgoing wave. The + means the wave travels in a positive direction and the—is just the opposite. μ means the coupling-loss between modes and η_in and η_on ($n = 1, 2$) represent, respectively, the internal loss and external loss of the corresponding mode. ω means the resonant angle frequency. Consequently, the equivalent complex amplitude can be expressed as follows

$$\begin{pmatrix} \eta_1 & -i\mu_{12} \\ -i\mu_{21} & \eta_2 \end{pmatrix} \cdot \begin{pmatrix} M_1 \\ M_2 \end{pmatrix} = \begin{pmatrix} \sqrt{\frac{1}{\eta_{o1}}} & 0 \\ 0 & \sqrt{\frac{1}{\eta_{o2}}} \end{pmatrix} \cdot \begin{pmatrix} M_{1+}^{in} + M_{1-}^{in} \\ M_{2+}^{in} + M_{2-}^{in} \end{pmatrix}, \tag{5}$$

$$\eta_n = (i\omega - i\omega_n - \eta_{\text{in}} - \eta_{\text{on}}). \tag{6}$$

Besides, the incident and outgoing waves of each coupling resonator should obey the energy conservation.

$$\begin{cases} \mathrm{M}_{n+}^{\text{in}} = \mathrm{M}_{(n-1)+}^{\text{out}} e^{i\phi_{n-1}} \\ \mathrm{M}_{(n-1)+}^{\text{in}} = \mathrm{M}_{n-}^{\text{out}} e^{i\phi_n} \end{cases} (n = 2) \qquad \begin{cases} \mathrm{M}_{n+}^{\text{out}} = \mathrm{M}_{n+}^{\text{in}} - \eta_{\text{on}}^{1/2}\mathrm{M}_n \\ \mathrm{M}_{n-}^{\text{out}} = \mathrm{M}_{n-}^{\text{in}} - \eta_{\text{on}}^{1/2}\mathrm{M}_n \end{cases} (n = 1, 2) \tag{7}$$

In the equation of conservation of energy, φ denotes the phase shift between two modes. Thus, we can use the following two formulas to calculate the transmittance of the system

$$\begin{cases} t = \dfrac{M_{2+}^{\text{out}}}{M_{1+}^{\text{in}}} \\ T = |t^2| \end{cases} \tag{8}$$

In addition, because the structure is composed of two orthogonal layers of grating that the output will be the same under TE and TM polarization. The total transmittance can be derived from the formula [39]

$$\begin{aligned} T &= T_{TM}T_{TE}\sum_{n=0}^{\infty}[(1 - T_{TM})(1 - T_{TE})]^n \\ &= \frac{T_{TM}T_{TE}}{[1 - (1 - T_{TM})(1 - T_{TE})]}. \end{aligned} \tag{9}$$

To verify the degree of agreement between the CMT theory and the results obtained from the numerical simulation, we compared the transmission spectra and CMT fitting data about the geometric parameters of

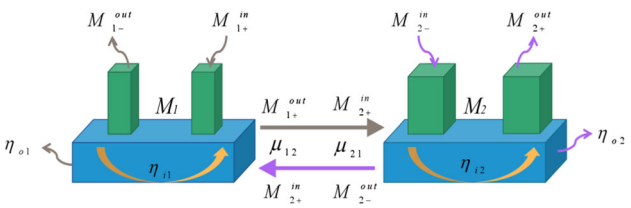

Fig. 2 Theoretical equivalent model of graphene grating coupling mode

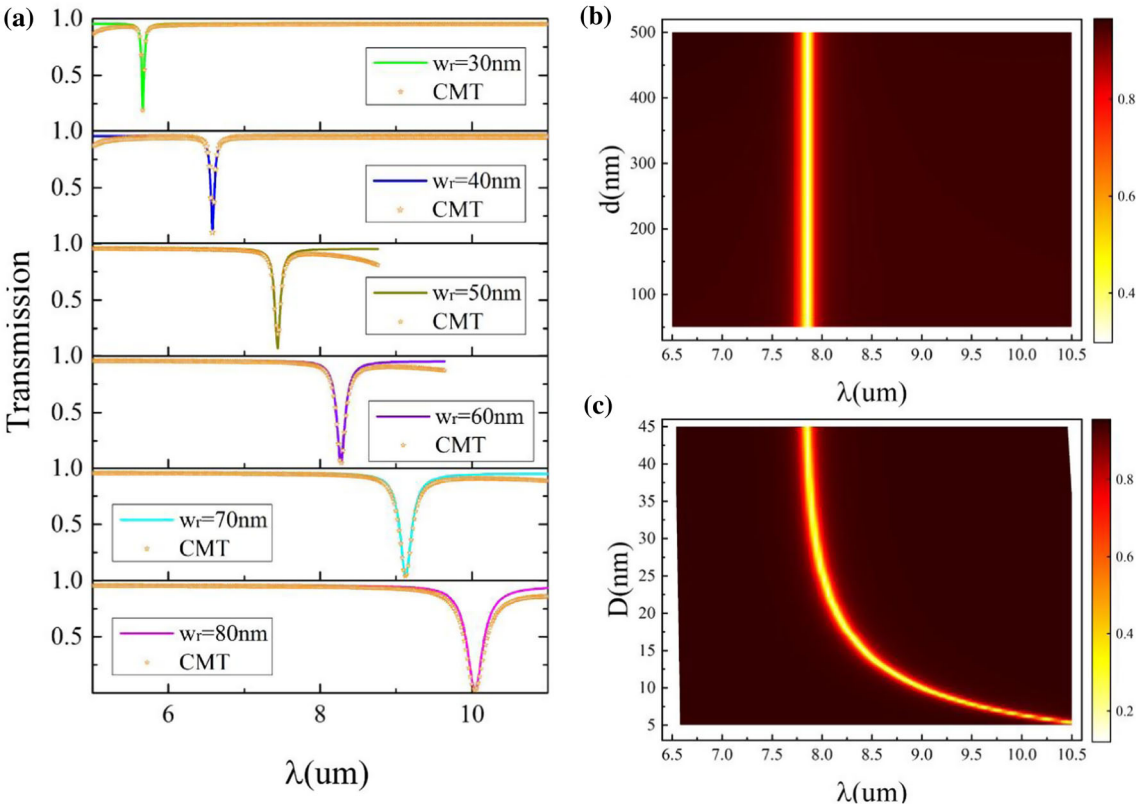

Fig. 3 **a** Transmission spectra of geometric parameters fitted with numerical simulation results and CMT. **b** Two-dimensional diagram of transmission spectrum of graphene grating structure with grating height d and **c** substrate thickness D

the graphene grating. Here we first change the geometric parameters of the first layer of graphene grating. Graphene is kept under the grating and its Fermi energy remains unchanged. Figure 3a illustrates the effect of changing the geometric parameters of the grating structure on the spectrum. As for TM polarization, when the width of the first layer grating increases in a step of 10 nm, the transmission spectrum presents a distinct red shift and the transmission valley gradually tends to zero as well. It can also be seen from the figure that the CMT theory is in good agreement with the numerical simulation results.

Other prominent geometric parameters are the depths of grating and substrate. Since the mode conversion occurs in the lower grating, we study the lower grating and set the Fermi energy of the lower grating to 1.0 eV. However, it is found that the transmission valley does not change measurably when the grating depth is changed, which is depicted in Fig. 3b. This feature makes the structure available to any system in spite of the height of the grating. Moreover, when the substrate thickness is more than 45 nm, no matter how much the change degree, the shift of transmission spectrum is extremely subtle. Figure 3c explains the relationship between substrate thickness in the range of 0–45 nm and transmission spectrum. When the substrate thickness D is less than 45 nm, the transmission peak of the spectrum produces an obvious blue shift with D increasing.

3 Results and discussion

It is found that when the grating width changes, the broadband transmission peak and the narrow band transmission peak are generated, as shown in Fig. 3a. To realize the low loss filtering function, we hope to find an optical band that satisfies the wide and narrow grating filtering at the same time. Set a wide grating width of 90 nm, narrow grating width of 45 nm. According to the dynamic tunability of graphene, adjust the Fermi energy of the continuous graphene layer at the bottom of the wide and narrow gratings, respectively. The results are proved in Fig. 4a and b. The lower the peak position, the better the filtering effect of the grating. Clearly, the narrow peak has the best filtering effect when the Fermi level is 0.6 eV, which transmittance is only 0.05. The transmission band of the narrow grating is between 6 and 9 μm and that of the wide grating is between 7.5 and 9.5 μm. It turns out to be that there are two corresponding wavelengths in these sets of data which make the two gratings have lower transmittance simultaneously. Setting the Fermi energy of narrow grating to 0.4 eV and the Fermi energy of wide

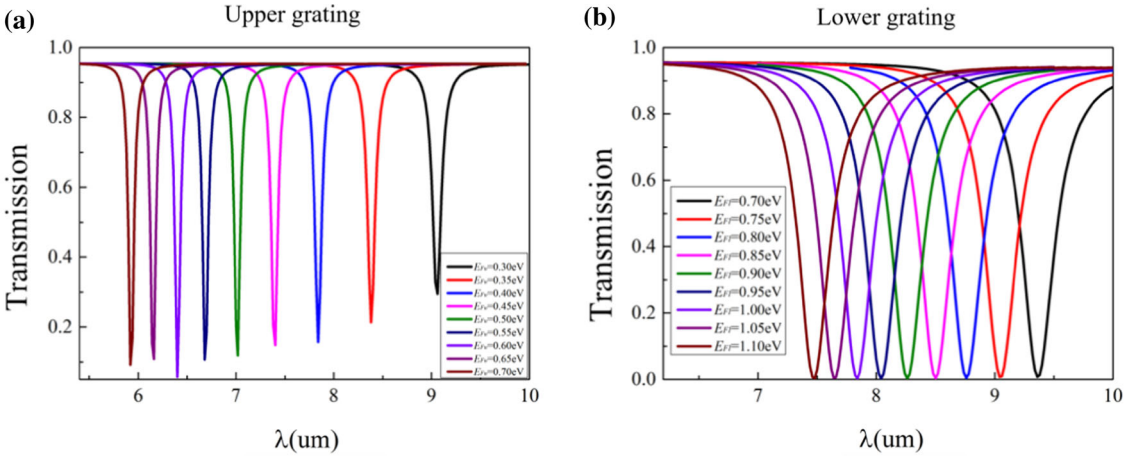

Fig. 4 The transmission spectrum of graphene grating system for different Fermi energy of **a** upper grating; **b** lower grating

grating to 1.0 eV, or setting the Fermi energy of narrow grating to 0.3 eV and the Fermi energy of wide grating to 0.75 eV, TM polarization can convert into TE polarization. We come to the conclusion that if the above two layers of gratings are superimposed into a composite grating, the filtering can be realized perfectly.

The narrow grating is placed over the wide grating, forming an angle of 90°. The core of the system is the effect of graphene on the hypersurface resonance filtering. The single-peak filtering spectrum is regulated by controlling the Fermi energy of graphene. Figure 5 depicts the transmission spectra of the gratings under TM polarization obtained by FEM. When the Fermi energy below the narrow grating is 0.4 eV, the Fermi energy of graphene below the wide grating is 1.0 eV, the transmission valley is formed at 7.83 μm concurrently and TM-polarized wave is converted into TE-polarized wave via two-layer gratings. Continuously adjust the Fermi level of graphene. It is found that when the Fermi energy shift to a low energy position, the transmission spectrum under TM polarization shows a significant red shift. When the graphene Fermi energy of narrow grating is 0.3 eV, the graphene Fermi energy of wide grating is 0.75 eV, a new transmission valley was formed at 9.05 μm as shown in Fig. 5b. It can be assumed that if the Fermi level is constantly changed, the structure can form a series of interval transmission valleys. The optical properties of the system are simulated by the finite element method, and the simulation results are completely consistent with the theoretical analysis.

For the single-peak broadband filter structure of applied metamaterials, the polarization angle and incident angle of the incident light wave are very crucial to its transmission spectrum. To test the performances of the system, we discuss the effect of the incident angle and polarizing angle on the transmission valley. Figure 6a explains the effect of the polarization angle on the filtering characteristics [40]. The figure shows the variation of the transmission of the filter with the polarization angle under the vertical incident condition of the incident light. It can be seen that when the polarization angle of the incident light wave changes from 0 to 90°, the transmission curve remains highly consistent, and the bandwidth and resonance frequency has no clear change. In fact, the polarization-independent properties of the filter are mainly attributed to the symmetry in the unit structure, that is, the upper and lower gratings are completely consistent in structure and conversion characteristics. An induced field arises between the two layers of gratings, and when the decrease or increase in the excitation efficiency due to a change in the polarization angle is compensated by the lower grating [41]. The structure is robust under the vertical incident conditions, this feature makes the filtering characteristics very stable.

The numerical simulation results in Fig. 6b indicate that the structure has polarization insensitivity when the incident wave is incident vertically for the case of TM polarizing waves. In a wide incident angle range of up to 30 degrees, changes in resonant frequency and FWHM of transmission spectra are not apparent, this structure has the perfect filtering [42] characteristics. Therefore, the magnetic resonance excited by the system is also unaffected in this incident angle range. When the incident angle exceeds the range, due to the diffraction effects of gratings the filtering performance would be degraded sharply with the increase of the incident angle, and the FWHM change is more significant.

4 Conclusions

In conclusion, we construct a TM/TE polarization mode converter, which is composed of two orthogonal gratings with graphene covered at the bottom of the gratings. Due to the dynamic tunability of graphene, the structure realizes a single-peak filter with clean transmission nulls at 7.83 μm and 9.05 μm. The switch of TM and TE polarization is achieved by coupling between two layers of graphene gratings in the same direction of the incident wave, which can be illustrated

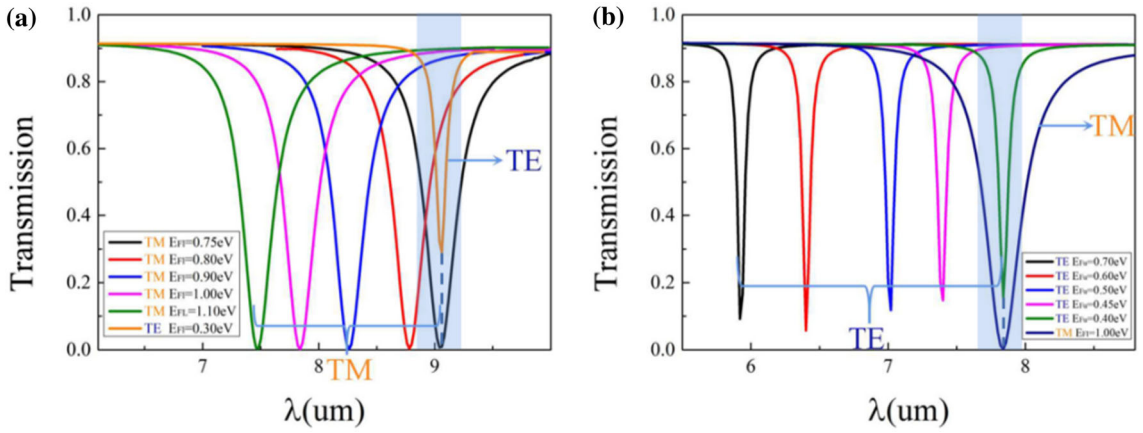

Fig. 5 The conversion diagram of TM polarization and TE polarization of the graphene grating system for different Fermi energy

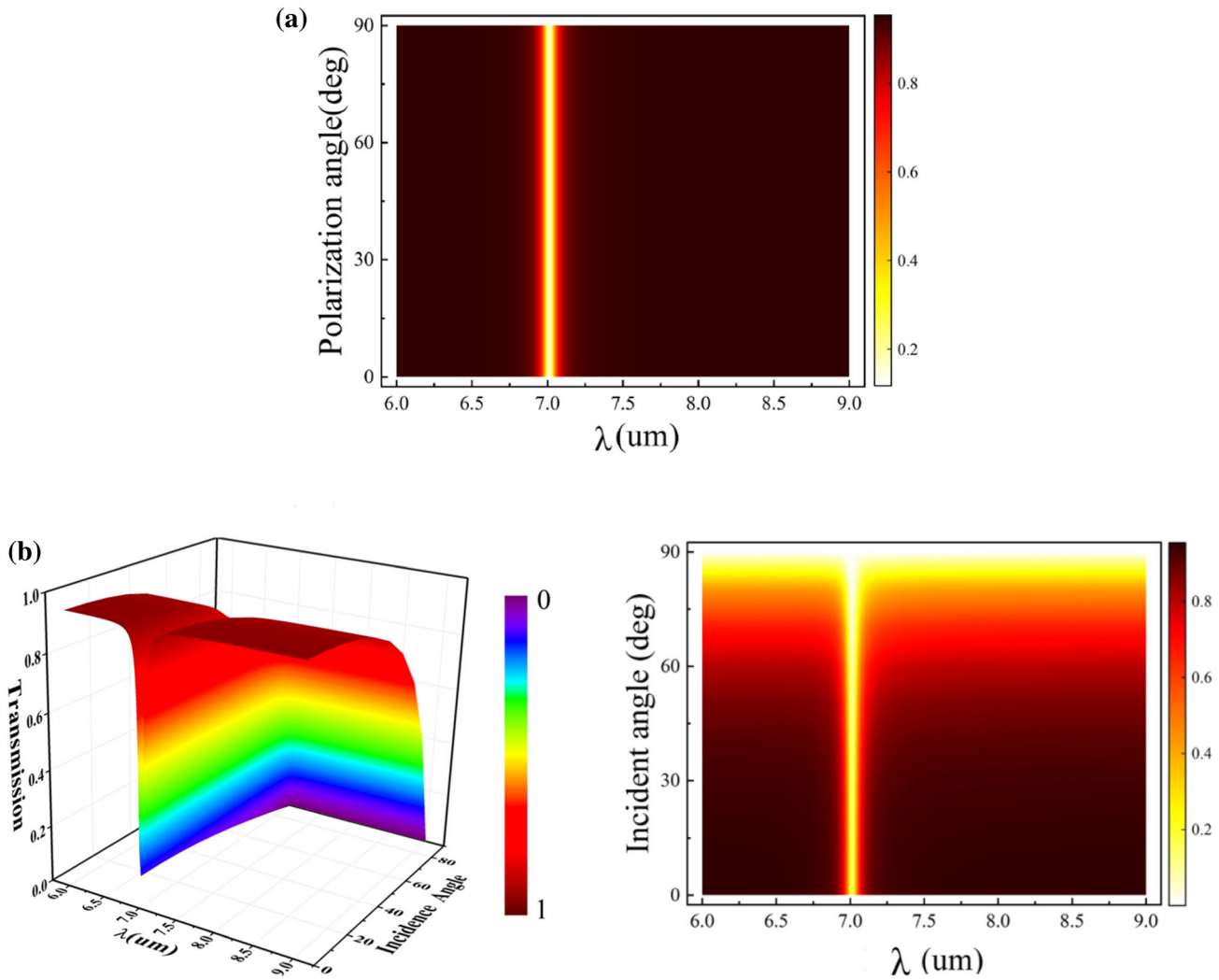

Fig. 6 The transmission spectrum as a function of **a** polarization angle and **b** incident angle for the TM polarization of the graphene grating system

by coupled-mode theory. The system has a wide application prospect because of its insensitivity in a small range of incident angle from 0 to 30°, polarization insensitivity and subtle size limitation. These features also provide a broader line of thought for the application of metamaterials such as perfect absorption and polarization conversion.

Acknowledgements This work is supported by the National Natural Science Foundation of China (11811530052); Intergovernmental Science and Technology Regular Meeting Exchange Project of Ministry of Science and Technology of China (CB02-20); Open Fund of State Key Laboratory of Applied Optics (SKLAO2020001A04); Undergraduate Research and Innovation Projects of Jiangnan University (2020366Y).

References

1. V. Mittal, N.P. Sessions, J.S. Wilkinson, G.S. Murugan, Opt. Mater. Express **7**, 712–725 (2017)
2. J. Wang, L. Sun, Z.D. Hu, X. Liang, C. Liu, AIP Adv. **4**, 123006 (2014)
3. W. Wang, Z. Zhao, C. Guo, F. Shen, J. Sun, Z. Guo, IEEE Photonics J. **12**, 4501108 (2020)
4. X.Y. Ding, Q.L. Kang, K. Guo, Z.Y. Guo, Opt. Mater. **109**, 110284 (2020)
5. K. Guo, H.S. Xu, Z.Y. Peng, X. Liu, Z.Y. Guo, IEEE Sens. J. **19**, 3654–3659 (2019)
6. O. Jafari, S. Zhalehpour, W. Shi, S. LaRochelle, Photon. Res. **9**, 471 (2021)
7. Q. Fan, M. Liu, C. Yang, L. Yu, F. Yan, T. Xu, Appl. Phys. Lett. **113**, 201104 (2018)
8. G. Brunetti, D. Conteduca, F. Dell'Olio, C. Ciminelli, M.N. Armenise, Opt. Express **26**, 4593 (2018)
9. M.D. Goldflam, Z. Fei, I. Ruiz, S.W. Howell, P.S. Davids, D.W. Peters, T.E. Beechem, Opt. Express **25**, 12400 (2017)
10. H.P. Zhou, L. Chen, F. Shen, K. Guo, Z.Y. Guo, Phys. Rev. Appl. **11**, 024046 (2019)
11. J.S. Gómez-Díaz, J. Perruisseau-Carrier, Opt. Express **21**, 15490 (2013)
12. T. Wang, M. Cao, H. Zhang, Y. Zhang, Appl. Opt. **57**, 9555 (2018)
13. S. Liu, H.B. Chen, T.J. Cui, Appl. Phys. Lett. **106**, 4918289 (2015)
14. A.V. Zayats, I.I. Smolyaninov, A.A. Maradudin, Phys. Rep. **408**, 131–314 (2005)
15. M.D. Goldflam, I. Ruiz, S.W. Howell, J.R. Wendt, M.B. Sinclair, D.W. Peters, T.E. Beechem, Opt. Express **26**, 8532–8541 (2018)
16. C. Sun, Z.W. Dong, J.N. Si, X.X. Deng, Opt. Express **25**, 1242–1250 (2017)
17. X. Duan, S. Chen, H. Cheng, Z. Li, J. Tian, Opt. Lett. **38**, 483–485 (2013)
18. M. Liu, X. Yin, E. Ulin-Avila, B. Geng, T. Zentgraf, L. Ju, F. Wang, X. Zhang, Nature **474**, 64–67 (2011)
19. L. Ju, B. Geng, J. Horng, C. Girit, M. Martin, Z. Hao, H.A. Bechtel, X. Liang, A. Zettl, Y.R. Shen, F. Wang, Nat. Nanotechnol. **6**, 630–634 (2011)
20. F.A. Vallejo, L.M. Hayden, Opt. Express **21**, 5842–5858 (2013)
21. F.M. Pigozzo, D. Modotto, S. Wabnitz, Opt. Lett. **37**, 2244–2246 (2012)
22. P. Bienstman, *Rigorous and efficient modeling of wavelength scale photonic components* (Universiteit Gent, 2001)
23. J.S. Gómez-Díaz, M. Esquius-Morote, J. Perruisseau-Carrier, Opt. Express **21**, 24856–24872 (2013)
24. F.H. Koppens, D.E. Chang, F.J.G. de Abajo, Nano Lett. **11**, 3370–3377 (2011)
25. X. Zhao, L. Zhu, C. Yuan, J. Yao, Opt. Lett. **41**, 5470–5473 (2016)
26. T.R. Bai, T. Yang, Z.D. Hu, T.L. Xing, Z.Y. Lu, Y.L. Huang, J.C. Wang, IEEE Sens. J. **21**, 2791–2797 (2021)
27. Y.C. Wang, T.T. Fernandez, N. Coluccelli, A. Gambetta, P. Laporta, G. Galzerano, Opt. Express **25**, 25193–25200 (2017)
28. S. Vasilyev, I. Moskalev, M. Mirov, V. Smolski, S. Mirov, V. Gapontsev, Opt. Mat. Express **7**, 2636–2650 (2017)
29. G.W. Hanson, J. Appl. Phys. **104**, 084314 (2008)
30. H.J. Li, L.L. Wang, B. Sun, Z.R. Huang, X. Zhai, J. Appl. Phys. **116**, 824 (2014)
31. J.H. Ge, C.L. You, H. Feng, X.M. Li, M. Wang, L.F. Dong, G. Veronis, M.J. Yun, Opt. Express **28**, 31781–31795 (2020)
32. D. Svintsov, V. Ryzhii, A. Satou, T. Otsuji, V. Vyurkov, Opt. Express **22**, 19873–19886 (2014)
33. H. Xu, H.J. Li, B. Li, Z.H. He, Z.H. Chen, M.F. Zheng, Sci. Rep. **6**, 30877 (2016)
34. J. Xu, H.W. Ruan, Y. Liu, H.J. Zhou, C.H. Yang, Opt. Express **25**, 27234–27246 (2017)
35. S. Popoff, G. Lerosey, M. Fink, A.C. Boccara, S. Gigan, Nat. Commun. **1**, 81 (2010)
36. H.A. Haus, W. Huang, Proc. IEEE **79**, 1505–1518 (1991)
37. K.R. Hiremath, J. Niegemann, K. Busch, Opt. Express **19**, 8641–8655 (2011)
38. Z.Y. Bao, J.C. Wang, Z.D. Hu, A. Balmakou, S. Khakhomov, Y. Tang, C.L. Zhang, Opt. Express **27**, 31435–31445 (2019)
39. K.J. Lee, Y.H. Ko, N. Gupta, R. Magnusson, Opt. Lett. **45**, 4452–4455 (2020)
40. W.J. Fang, C.Y. Yue, X.Y. Fan, H.H. Niu, X. Zhang, H.Y. Xu, N.K. Chen, C.L. Bai, Asia Commun. Photonics Conf. **10**, 8595906 (2018)
41. S.X. Xia, X. Zhai, L.L. Wang, S.C. Wen, Photonics Res. **6**, 692–702 (2018)
42. A.R.S. Lins, J.R.F. Lima, ISSN **160**, 353–360 (2020)